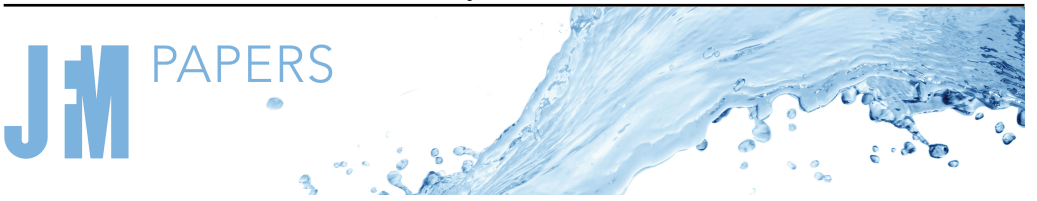
J. Fluid Mech. (2025), *vol.* 1024, A36, doi:10.1017/jfm.2025.10840



Steady advection–diffusion in polygonal microfluidic mixers

Etienne Boulais[1], **Aniket Udepurkar**[1], **Cedric Devos**[1], **Martin Z. Bazant**[1,2], **Allan S. Myerson**[1] **and Richard D. Braatz**[1]

[1]Department of Chemical Engineering, Massachusetts Institute of Technology, 77 Massachusetts Avenue, Cambridge, MA 02139, USA

[2]Department of Mathematics, Massachusetts Institute of Technology, 77 Massachusetts Avenue, Cambridge, MA 02139, USA

Corresponding author: Richard D. Braatz, braatz@mit.edu

(Received 4 April 2025; revised 28 August 2025; accepted 5 October 2025)

We present theoretical models for flow and diffusion in microfluidic polygonal mixers of arbitrary shapes. Combining work based on Boussinesq coordinates with modern methods for the calculation of the Schwarz–Christoffel transform, we present an integrated method that yields analytical solutions for both flow and concentration profiles everywhere in microfluidic mixers with arbitrary numbers of inlets. We illustrate how the problem can be reduced to a sequence of conformal maps to a known domain, where the advection–diffusion problem can be readily solved, and map back the solution to the geometry of interest. We use the method to model a number of previously published microfluidic mixer geometries, used in lipid nanoparticle synthesis, among others. The method is also applicable to other problems described by planar transport equations in polygonal domains, for instance, in groundwater flows or electrokinetics.

Key words: Hele-Shaw flows, coupled diffusion and flow, microfluidics

1. Introduction

Passive micromixers were one of the first element to be added to the microfluidic toolbox. Early systems, such as T-mixers (Kamholz *et al.* 1999), H-filters (Brody & Yager 1997) and hydrodynamic focusing chips (Knight *et al.* 1998), were used for the design of separation systems (Weigl & Yager 1999), diffusion-based assays (Hatch *et al.* 2001) and controlled chemistry at interfaces (Atencia & Beebe 2005). These systems usually operate at high Péclet numbers and exchange between the different incoming streams happens by slow, linear diffusion. As rapid mixing equipment, these simpler systems were eventually replaced by chaotic mixers (Stroock *et al.* 2002), which use 'stretch-and-fold' dynamics

© The Author(s), 2025. Published by Cambridge University Press.

https://doi.org/10.1017/jfm.2025.10840 Published online by Cambridge University Press

to enact mixing in time scales orders of magnitude more rapid than passive diffusion (Ottino & Wiggins 2004).

In recent years, however, there has been a renewal of interest for more complex system geometries that still exhibit passive advection–diffusion, free of chaotic features. In pharmaceutical applications, devices based on variants of hydrodynamic focusing chips have been used as tools for the synthesis of complex lipid particles, first liposomes (Jahn *et al.* 2007; van Swaay & DeMello 2013), then lipid nanoparticles (Krzysztoń *et al.* 2017). The synthesis of these particles is typically done using rapid solvent–antisolvent mixing, where an organic stream containing precursor lipids is rapidly mixed with an aqueous stream containing payload molecules (Buschmann *et al.* 2021). A current active area of research in the field is the precise determination of process-property parameters (Devos *et al.* 2024) and the mixing equipment is known to have an important impact on final product characteristics, as shown by the few systematic studies investigating similar formulations with different mixers (O'Brien Laramy *et al.* 2023; Petersen *et al.* 2023; Chen *et al.* 2025). Formation of liposomes and other small lipid vesicles is known to be a kinetic, non-equilibrium process (Leng, Egelhaaf & Cates 2003). As such, simple equilibrium considerations (Lasic *et al.* 2001) are inadequate in predicting output, and a detailed knowledge of the microenvironment history of individual lipid nanoparticles during their formation is necessary for a correct prediction of their final morphology. Microfluidic mixers offer a unique opportunity to probe these complex self-assembly mechanisms. Flow and concentration gradients within them are much more regular and predictable than in their chaotic or turbulent counterparts. This makes the precise determination of the flow and concentration everywhere within them feasible. This regularity allows for the probing of the microenvironment of nucleating particles with a granularity that is impossible in larger mixers. Low-enough-Reynolds-number mixers have the advantage of being amenable to analytic treatment, which can considerably speed up calculations and give insight into scaling behaviour that would otherwise be laborious to obtain from numerical studies. There is a clear need for precise analytical models of transport in these microfluidic mixers. Such models should give us complete information about flow and diffusion in experiments, such as the solvent–antisolvent precipitation used in nanoparticle formation, and be applicable to the wide range of mixer geometry that currently exists.

Problems of complex planar flow have a long history of analytical treatment. Potential flow theory, combined with complex variable methods, has been a mainstay of theoretical hydrodynamics, from the pioneering work of Lamb (1924) and Milne-Thomson (1943), to its application to planar Darcy flows, omnipresent in groundwater mechanics (Strack 1988). Methods based on conformal transforms have also been used to study other transport problems associated with these flows. Starting with Boussinesq (1902), it has been known that advection–diffusion in planar potential flow is conformally invariant. Similar transformations to that used by Boussinesq were later applied to the study of turbulent dispersion of pollution by wind (Hunt 1973; Hunt & Mulhearn 1973), to tracer dispersion in porous media (Koplik, Redner & Hinch 1994), to solidification problems (Cummings *et al.* 1999) and to dispersion by bluff bodies (Eames & Bush 1999), just to name a few. Work by Martin Bazant in the 2000s showed how the Boussinesq problem was a specific example of a wider family of conformally invariant systems (Bazant 2004) and later applied the method to problems of non-Laplacian growth (Choi *et al.* 2005), as well as the elaboration of three-dimensional (3-D) solutions of the Navier–Stokes equation (Bazant & Moffatt 2005). The same methodology was used to study induced recirculation in problems of magnetohydrodynamics in the Hele-Shaw cell (McKee 2024). More recently, conformal mapping techniques have been applied to the determination of a steady-state concentration profile in a range of planar microfluidic systems. Arrangement

https://doi.org/10.1017/jfm.2025.10840 Published online by Cambridge University Press

of point sources and sinks have been used to study complex staining over surfaces (Goyette *et al.* 2019) and were subsequently shown to apply to large families of microfluidic systems (Boulais & Gervais 2023). Similar flow and concentration patterns were simultaneously found to appear in the human choriocapillaris (Zouache, Eames & Luthert 2015). Diffusion in channel junctions, such as T-sensors and hydrodynamic focusing chips, was studied using a combination of simplified semi-infinite channel geometry, and careful arrangements of point sources and sinks (Boulais & Gervais 2020).

In this article, we extend this previously published body of work and present a theoretical framework for analysis of flow and diffusion in arbitrarily shaped microfluidic mixers. While previously cited work has focused on simple geometries (either radially symmetrical or based on simple rectangular channels), the method proposed here is applicable to mixers and channel junctions of arbitrary polygonal shapes, which is more representative of real mixing equipment. The method yields the exact concentration everywhere in the mixer, allowing for precise determination of the microenvironment history of individual particles, a crucial missing ingredient in the search for better models of self-assembly of lipid nanoparticles. The method presented here is based on the use of Schwarz–Christoffel maps (Driscoll 2002), which have been known in the applied mathematics community for a long time, but have found very little applications in microfluidics and in pharmaceutical applications. Schwarz–Christoffel maps enabled the resolution of flow problems in complex channels (Floryan 1985), of general free surface flow problems (Dias, Elcrat & Trefethen 1987) as well as problems of flow in porous media (Smith 1996), but have been comparatively much less used in analysing the associated advection–diffusion problem that comes with these flows.

Using a sequence of conformal maps, we reduce the problem of advection–diffusion in a polygonal mixer to a known geometry and formulate an analytical solution for the velocity as well as the concentration profile everywhere in the mixer. One crucial map in the sequence, the map from an arbitrary polygon, has a set of unknown real parameters that need to be computed numerically. The method is thus semi-analytical. Since the map to and from the polygonal geometry only has to be computed once (as the mixer geometry does not change from one experiment to the next), the method allows for near instant determination of the concentration field and velocity, which could enable its use in control applications, where execution speed is often crucial. We focus here on microfluidic systems, given the comparatively more simple and regular characteristics of their flow and transport. Since flow in such systems can be kept laminar and free from chaotic features, they allow in principle a complete determination of flow and diffusion within them from knowledge about their input parameters (incoming flow rates, device dimensions, diffusion coefficients of components, etc.). However, the method of mapping shown here can also be used to generate grids that can serve as a starting point for efficient numerical analysis of more complex chaotic flows (Floryan 1985). Once we have outlined the models and shown how they can be used to analyse mixers of arbitrary geometries, we then move on to compare predicted results with experimental physical tracer tests.

2. Theory

2.1. *Problem description*

We are looking for a complete description of velocity and concentration profiles within a polygonal microfluidic mixer such as illustrated in figure 1. Such mixers typically have two or more inlets and a single outlet. In a typical flash nanoprecipitation experiment, the inlets will inject either solvent or antisolvent, the mixing of which we model using

https://doi.org/10.1017/jfm.2025.10840 Published online by Cambridge University Press

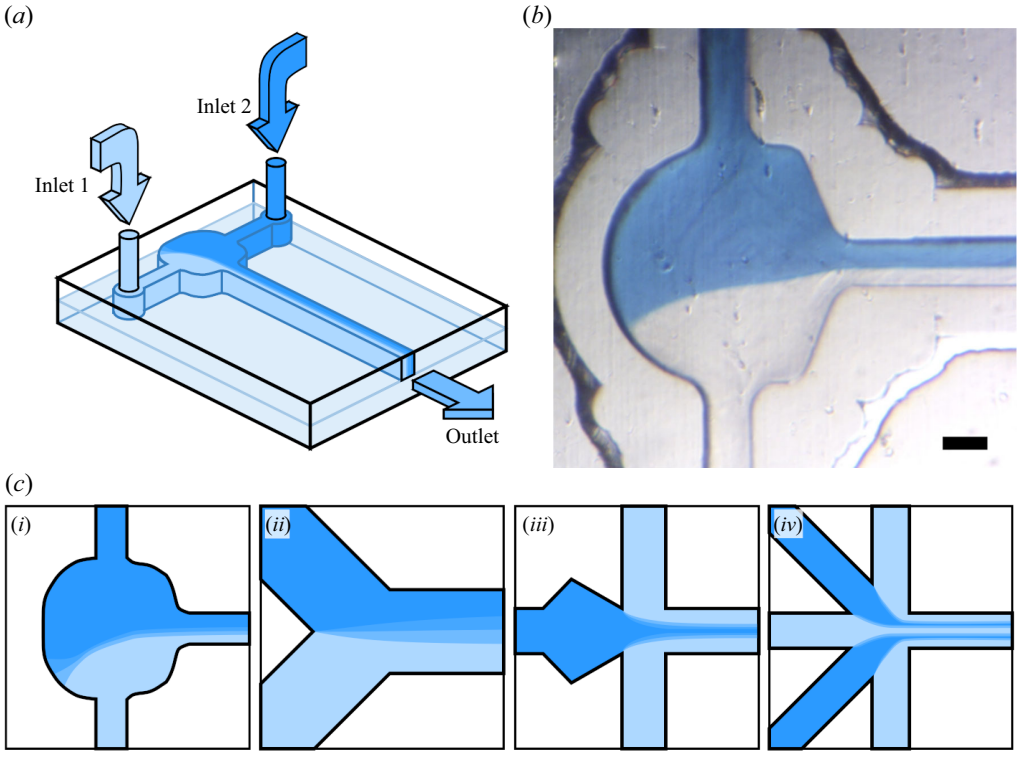


Figure 1. Microfluidic mixer geometry. (*a*) Schematic of the mixer. (*b*) Experimental picture of a physical tracer test in a microfluidic impinging jet mixer (scale bar, 100 μm). (*c*) Different types of mixer geometries that have been published: (*i*) microfluidic analogue to an impinging jet mixer; (*ii*) Y-junction (Gobby, Angeli & Gavriilidis 2001); (*iii*) hydrodynamic focusing system (Knight *et al.* 1998); (*iv*) multi-inlet hydrodynamic focusing (Park *et al.* 2006).

linear advection–diffusion. In some experiments, inlets may also have different initial temperatures, leading to temperature gradients on top of concentration gradients. As a first approximation, temperature gradients may also be modelled using linear advection–diffusion, but doing so neglects heat of mixing, which may become important in experiments involving the mixing of alcohol and water as solvent and antisolvent (Peeters & Huyskens 1993). Linear models may thus be applicable in cases where the difference in temperature between inlets is already much bigger than the difference in temperature generated by the heat of mixing. As a first approximation, we will suppose the Reynolds number to be low enough for creeping flow approximations to hold. This is adequate for typical hydrodynamic focusing systems (Knight *et al.* 1998; Jahn *et al.* 2007), where rapid mixing is achieved by controlling the inlet ratio. This type of approximation breaks down for systems where inertial effects and chaotic mixing become important. We are focusing on quasi-planar geometries, where the mixer's height is uniform and comparatively smaller than the other dimensions of the problem. This is consistent with standard methods of microfluidic system fabrication, and allows us to treat the problem as a quasi-two-dimensional (quasi-2-D) problem, which is common of many complex microfluidic flows (Boulais & Gervais 2023).

The method presented here allows for an arbitrary number of inlets and outlets, with each inlet fixed at a known concentration. Typical microfluidic mixers for nanoparticle synthesis may exhibit two (Hatch *et al.* 2001; Devos *et al.* 2024), three (Knight *et al.* 1998) or a larger number of inlets (Park *et al.* 2006).

https://doi.org/10.1017/jfm.2025.10840 Published online by Cambridge University Press

2.2. *Constitutive equations*

The equations describing the flow are the incompressible Navier–Stokes equation. If the depth of the mixer's chamber is much smaller than the characteristic length in the horizontal direction, then the flow in the mixer can be adequately described as a Hele-Shaw cell. In that case, the Navier–Stokes equations reduce to the Hele-Shaw equations, which are easily solved for the in-plane velocity components (Batchelor 2000),

$$u \approx -\frac{1}{2\mu}\frac{\partial p}{\partial x} z(d-z), \qquad v \approx -\frac{1}{2\mu}\frac{\partial p}{\partial y} z(d-z), \tag{2.1}$$

where μ is the viscosity of the fluid, d the depth of the chamber and p is the hydrostatic pressure. Equation (2.1) can be rewritten as

$$\boldsymbol{u} = -\nabla\phi(x, y) z(d-z), \tag{2.2}$$

which is the product of a parabolic flow in the z direction and the gradient of a 2-D potential function in the xy plane. Combining (2.1) with the continuity equation $\nabla \cdot \boldsymbol{u} = 0$ yields the 2-D Laplace equation for our potential function $\phi(x, y)$,

$$\nabla^2 \phi = 0. \tag{2.3}$$

The solution of (2.3), combined with (2.2), gives us complete information of our flow field. This is valid as long as the Reynolds number is reasonably small and that the main features of the flow happen sufficiently far from the wall, as the potential flow formulation breaks down at a distance from the wall comparable to the channel height (Gökçe *et al.* 2019). Tracer dispersion in the mixer can be described by the steady-state linear advection–diffusion equation,

$$0 = \nabla^2 c - Pe\, \boldsymbol{u} \cdot \nabla c, \tag{2.4}$$

where $Pe = (Q_0/2\pi G D)$ is the Péclet number, representing the ratio of advective to diffusive transport, with Q_0 being a characteristic flow rate, G is the thickness of the Hele-Shaw cell in the z direction and D is the diffusion coefficient of the tracer. We take Q_0 as the flow rate of one of the inlets. From the characteristic flow rate Q_0, a characteristic velocity u_0 can be obtained,

$$u_0 = \frac{Q_0}{2\pi L G}, \tag{2.5}$$

where L is a characteristic dimension in the xy plane, which we usually take to be the width of the outlet channel. Taking the depth-averaged concentration field in the chamber, the concentration field is described by the 2-D advection–diffusion equation,

$$0 = \nabla^2 c - Pe \nabla\phi \cdot \nabla c, \tag{2.6}$$

which is valid as long as the concentration field can be assumed to be relatively constant in the z direction. Caveats and limit cases for such an approximation are discussed further by Boulais & Gervais (2020). The same system of equation would also be valid in the case of a device extending infinitely in the z direction. When solving this 2-D flow and concentration problem, we prescribe slip boundary conditions for the flow, as well as no-flux conditions for the concentration field on the walls of the mixers. Inlets and outlets have prescribed inflow (or outflow), and a prescribed concentration at each inlet.

2.3. *Conformal mapping strategy*

The description of the problem in terms of 2-D potential flow strongly suggests the use of complex variable representation (Milne-Thomson 1943). The position vector can be

https://doi.org/10.1017/jfm.2025.10840 Published online by Cambridge University Press

rewritten in terms of a single complex variable $w = x + iy$. We can then write the complex potential $\Phi(w) = \phi + i\psi$ as a function of a single complex variable, with the real part ϕ corresponding to the level sets of the real potential and the imaginary part ψ corresponding to the streamlines of the flow. The components of the velocity field can be obtained from the complex potential by using the expression for the complex velocity,

$$u - iv = -\frac{\mathrm{d}\Phi}{\mathrm{d}w}, \tag{2.7}$$

or equivalently,

$$u = -\frac{\partial\phi}{\partial x} = -\frac{\partial\psi}{\partial y}, \qquad v = \frac{\partial\psi}{\partial x} = -\frac{\partial\phi}{\partial y}. \tag{2.8}$$

Formulation of the 2-D problem in terms of complex variable immediately enables us to use conformal maps, which are a standard tool in 2-D hydrodynamics (Lamb 1924; Milne-Thomson 1943; Strack 1988). More importantly, if the problem is formulated in this way, the associated advection–diffusion problem (2.6) is also conformally invariant (Boussinesq 1902; Bazant 2004). Our mixer has a complex irregular shape, which may reduce our hope for an analytical solution. However, maps from the half-plane to the interior of arbitrary polygons, called Schwarz–Christoffel maps, can in principle always be found, even though they may not have simple closed-form analytical expressions. Efficient numerical methods for computing such maps have been described in the past (Trefethen 1980) and applied to hydrodynamics problems (Elcrat & Trefethen 1986; Dias *et al.* 1987). While numerical methods for the computation of Schwarz–Christoffel methods have been around since the 1980s, their application to concrete transport problems have been relatively scarce. This lack of application could be due to the wider availability of direct numerical solvers for this kind of problem or to a perceived complexity of the method by wider engineering audiences. To the best of our knowledge, the current paper is the first report of an integrated method for analysing transport in microfluidic systems using Schwarz–Christoffel maps to arbitrary polygonal geometries.

2.4. *Sequence of transforms*

Since our system of equations is conformally invariant, solving the problem reduces to finding a sequence of conformal transforms that map our polygonal mixer domain to a simplified geometry in which flow and concentration can readily be solved. Such a sequence of maps is illustrated in figure 2. Keeping the notation for the different domains uniform with the existing literature is difficult, considering the number of intermediary steps in our derivation and the varying conventions across different sources. We use w for the interior of the mixer and z for the disk domain, so that the equations relating to the Schwarz–Christoffel transforms directly match the equations of Trefethen (1980). We write $\Phi = \phi + i\psi$ for the streamline domain to retain the standard ϕ and ψ for the hydrodynamic potential and stream function. The intermediate plane domain is written as ν as it is a variable name that is not easily confused with others in this paper and related works. This notation differs from older hydrodynamic texts such as Lamb (1924) and Milne-Thomson (1943), where the complex potential is usually written as $w = \phi + i\psi$.

We now describe each of the maps used to simplify the problem. The first, and arguably more complex step, is to map the complex polygonal shape of the mixer to a simpler domain, in this case, the interior of a disk. Maps from disks to polygons, known as

https://doi.org/10.1017/jfm.2025.10840 Published online by Cambridge University Press

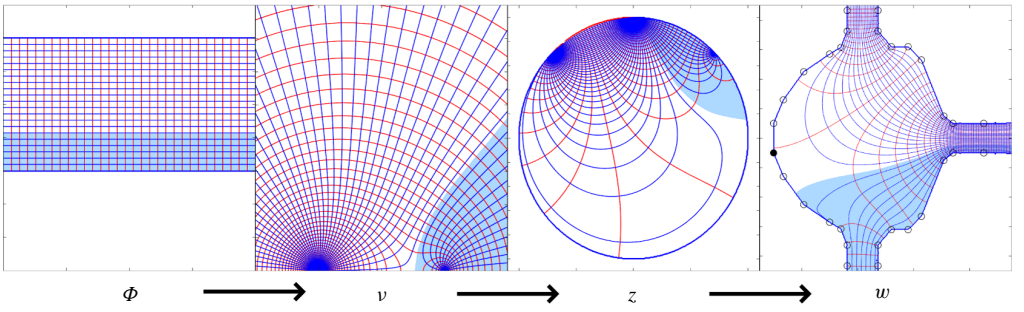


Figure 2. Sequence of transforms involved in going from the flat, streamline domain Φ to the mixer geometry w.

Schwarz–Christoffel maps, are given by Driscoll (2002),

$$w(z) = w_c + C \int^z \prod_{k=1}^{n} \left(1 - \frac{\xi}{z_k}\right)^{\alpha_k - 1} \mathrm{d}\xi, \tag{2.9}$$

where the α_k are the interior angles at each corner (expressed in multiples of π) and the z_k are the images of the vertices of the polygon in the disk domain, distributed along the circumference of the unit circle in the z domain. Such a domain, which has the geometry of a disk with point sources and sinks distributed around its circumference, has been used in the past to study chaotic mixing (Metcalfe *et al.* 2010) as well as in control applications (Schneider, Mandre & Brenner 2011). The value of the parameters z_k has to be determined as part of the solution procedure, see § 2.8 for more details. The introduction of an intermediate disk domain z ensures that the integrals are always computed in a bounded domain. This disk domain can be 'unwrapped' to the upper half-plane ν by using the Moebius transform,

$$\nu = i \frac{z + z_0}{z - z_0}, \tag{2.10}$$

where z_0 is the image of the outlet in the z domain to be determined as part of the solution procedure. This form of the map maps the circumference of the disk to the real axis, with the point z_0 being mapped to infinity in the ν domain. The flow problem can then directly be solved in the upper half-plane domain ν. In this domain, each of the inlets maps to a point source on the real axis. In this half-plane domain, the flow potential $\Phi(\nu)$ can be directly written as a superposition of logarithmic point sources,

$$\Phi(\nu) = \sum_i k_i \ln(\nu - \nu_i), \tag{2.11}$$

where the sum is over all inlets, k_i is the dimensionless flow rate of each inlet i ($k_i = 1$ corresponding to an inlet with dimensional flow rate Q_0) and ν_i is the image of the inlet i in the half-plane domain, to be determined as part of the solution procedure. At this point, the flow problem is solved. However, to solve the associated steady advection–diffusion problem, we need to use the map $\Phi(\nu)$ to the streamline coordinate domain, where the flow is a simple plane flow.

https://doi.org/10.1017/jfm.2025.10840 Published online by Cambridge University Press

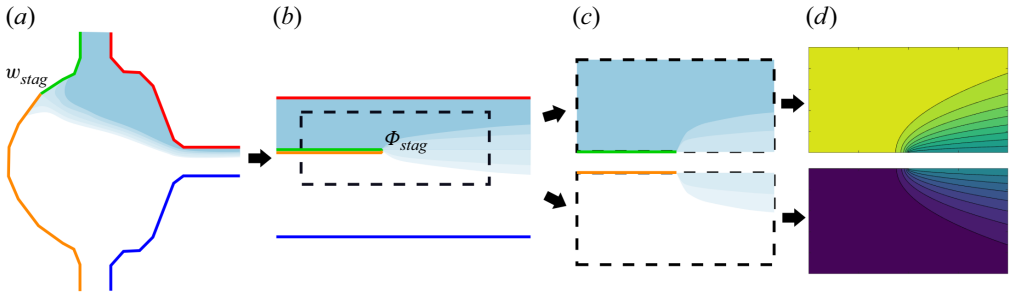


Figure 3. Illustration of the construction of the solution in the streamline domain. (*a*) Mixer geometry w. (*b*) Streamline coordinate domain problem. (*c*) Two halves of the streamline problem for high Pe, in which the outer walls are neglected. (*d*) Two leading edge similarity solutions to be patched together.

2.5. *Streamline coordinate domain*

In the streamline coordinate domain $\Phi = \phi + i\psi$, the steady advection–diffusion equation takes the form

$$\frac{\partial^2 c}{\partial \psi^2} + \frac{\partial^2 c}{\partial \phi^2} - Pe\frac{\partial c}{\partial \phi} = 0. \tag{2.12}$$

While the form of the equation is much simpler, in the general case, the problem in the streamline coordinate domain might have one or several mixed boundary conditions, which can be difficult to deal with. We first describe the construction of the solution for the simpler case of two inlets and one outlet.

In the problem of two inlets of unequal flow rates, the streamline coordinate problem maps to two strips of different concentrations, each with a height of $k_i\pi$. The strips are initially separated by a no-flux boundary which ends at a point Φ_{stag}, then allowed to mix with one another (see figure 3). The point Φ_{stag} corresponds to the image of the stagnation point located between the two point sources in the ν domain. This stagnation point's position is given by

$$\nu_{stag} = \frac{k_1\nu_2 + k_2\nu_1}{k_1 + k_2} \tag{2.13}$$

and its image in the Φ domain is

$$\Phi_{stag} = k_1 \ln(\nu_{stag} - \nu_1) + k_2 \ln(\nu_{stag} - \nu_2). \tag{2.14}$$

The presence of the mixed boundary condition separating the two strips significantly complicates the problem; however, in the case of high-Péclet-number flows, it is possible to cut up the problem into a number of simpler subdomains and use this subdivision to construct solutions which are valid everywhere. In a high-Péclet-number regime, the mixing region will be confined to a thin wake originating at Φ_{stag} and of thickness $\sqrt{(\phi - \phi_{stag})/Pe}$. As long as the thickness of this wake is small compared with the width $k_i\pi$ of the strip in the streamline domain, the effect of the no-flux boundaries at the top and bottom of the strip (red and blue segments in figure 3*b*) will be negligible. Neglecting the outer boundary conditions in the streamline domain, we are left with the problem of an infinite domain with a different prescribed value of c at infinity on each half-plane (dotted box in figure 3*b*). The two half-planes are separated by a semi-infinite no-flux boundary that ends at Φ_{stag}. In this subdomain, the problem is symmetrical and the concentration on the separating axis, past Φ_{stag}, can be taken to be just the average of the two inlet concentrations.

https://doi.org/10.1017/jfm.2025.10840 Published online by Cambridge University Press

We can finally split the problem into two simpler sub-problems (see figure 3*c*). In each 'half' of the subdivided problem, we have a problem of advection–diffusion in plane flow in a semi-infinite domain, with a symmetry condition on half of the real axis, a prescribed concentration of $c = 1/2$ on the other half of the real axis and a concentration that tends to either 0 or 1 as $|\Phi| \to \infty$. The problem has thus been reduced to the classical boundary layer for uniform flow past a semi-infinite slipping flat plate. This problem can be solved in parabolic coordinates and has a simple similarity solution in terms of error functions (Cummings *et al.* 1999; Bazant 2004). We can patch the two halves of the solution together to obtain an expression for the concentration field:

$$c\left(\Phi\right) = \begin{cases} \frac{1}{2}\left(1 - \operatorname{erf}\left(\operatorname{Im}\sqrt{Pe\left(\Phi - \Phi_{stag}\right)}\right)\right), & \psi < 0, \\ \frac{1}{2}\left(1 + \operatorname{erf}\left(\operatorname{Im}\sqrt{Pe\left(\Phi - \Phi_{stag}\right)}\right)\right), & \psi \geqslant 0. \end{cases} \tag{2.15}$$

This solution has the familiar square root scaling of boundary layer thickness for slipping plates, which would be recuperated by using classical boundary layer analysis. Such a method of patching solutions together that appear on opposite sides of a separating streamline has been done in the past by Bazant & Moffatt (2005) in constructing solutions to the Navier–Stokes equation with steady vortex structures. The novelty here lies in the shifting of the potential between the two half-plane solutions using Φ_{stag}. This shifting of the solutions becomes non-trivial when constructing more elaborate solutions where more than two subdomains are patched together, such as happens when analysing multiple inlets (see § 2.6). In that case, multiple stagnation points appear and different parts of the solution have their potential shifted by different values of Φ_{stag}.

The solution (2.15) breaks down when $\sqrt{(\phi - \phi_{stag})/Pe}$ becomes comparable to the strip width $k_i\pi$, at which point, the neglecting of the outer boundaries is no longer justified and the assumption that the separating line has a constant concentration, which is the average of the two inlet concentrations, is no longer true. In a previous publication, we have shown how a solution for this far-field regime can be obtained in terms of Green's functions (Boulais & Gervais 2020).

2.6. *Multiple inlets solution*

The procedure for solving the diffusion problem in mixers with more than two inlets is similar to the above-mentioned one, but involves a patching together of more than two similarity solutions. In multi-inlet mixers, the streamline domain Φ corresponds to a series of strips of different concentration, initially separated by boundaries across which concentration cannot pass, and put in contact at different points (see figure 4).

Like in the two-inlet case, identification of the stagnation points' image in the Φ domain is important, as they represent the end of the semi-infinite boundaries initially separating the different strips. There is a stagnation point in between each pair of point sources in the ν domain. While analytical determination of each stagnation point's position is cumbersome when there are more than two apertures, there are a number of simple ways to approximate their positions.

(i) Numerically solve the equation $\nabla\Phi(\nu) = \mathbf{0}$ to find the position of each stagnation point.
(ii) Use the weighed average of each pair of inlets to find the stagnation point between them. This assumes that the effect of the other inlets is mostly screened out by the two nearest singularities and the error committed in that case should be minimal.

https://doi.org/10.1017/jfm.2025.10840 Published online by Cambridge University Press

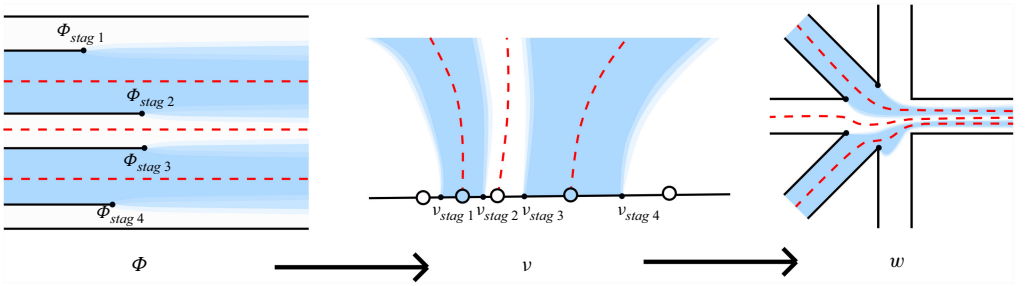


Figure 4. Schematic of the different domains involved in the multi-inlet problem (the intermediate disk domain z is not pictured). By slicing the domain along the red dotted lines, the problem can be subdivided into a sequence of smaller problems whose solution is given by (2.15). The solution breaks down when the wake's width becomes comparable to the distance between dotted lines, or to the width of the smallest strip segment.

(iii) If the mixer geometry has relatively sharp corners (such as illustrated in figure 8*c*) and the ratio of the different injection rates are not too big, we can approximate that the position of the stagnation point will correspond to the image of the corresponding corner.

The solution will be a patchwork of wakes, each translated by the position of their respective stagnation point.

2.7. *Multiple outlets*

The solution procedure gets more complicated if there are multiple outlets. In problems with multiple outlets, the fluids of different concentration can be put in contact for a finite distance, then reseparated. In such a geometry, the mixing region can be confined to a strip of finite length, requiring more complex solution procedures. Such a finite strip problem (Pearson 1957) has been studied using combinations of numerical and analytical methods in problems of solidification in potential flows (Choi *et al.* 2005). In microfluidics, classic H-filter systems (Weigl & Yager 1999) as well as microfluidic surface shields (Boyadjian, Boulais & Gervais 2022) involve such a streamline domain, where the finite strip solution needs to be used.

2.8. *Schwarz–Christoffel maps*

A key step in the derivation of our solution is the computation of the Schwarz–Christoffel map 2.9 between the complex polygonal mixer and disk domain. This map has a number of unknown z_k parameters, which are the images of the vertices of the polygon in the disk domain, distributed along the circumference of the unit circle in the z domain. With the exception of some limited cases with small numbers of vertices or high symmetry, the integral in (2.9) usually does not have a closed expression in terms of simple functions. However, its value at any point in the domain can easily be computed using numerical quadratures. The main difficulty in computing (2.9) is in determining the set of parameters z_k, which is usually called the 'parameter problem', and is the more laborious part in computing complex Schwarz–Christoffel maps. The parameters z_k are not known *a priori* and have to be determined by numerically solving a nonlinear system of equation, based on the constraints of our geometry. The method is in that sense semi-analytical. Various numerical methods for the generation of Schwarz–Christoffel maps (and the resolution of the parameter problem) have been presented throughout the years (Menikoff & Zemach 1980; Stephenson 2005; Marshall & Rohde 2007); this work implements the method

https://doi.org/10.1017/jfm.2025.10840 Published online by Cambridge University Press

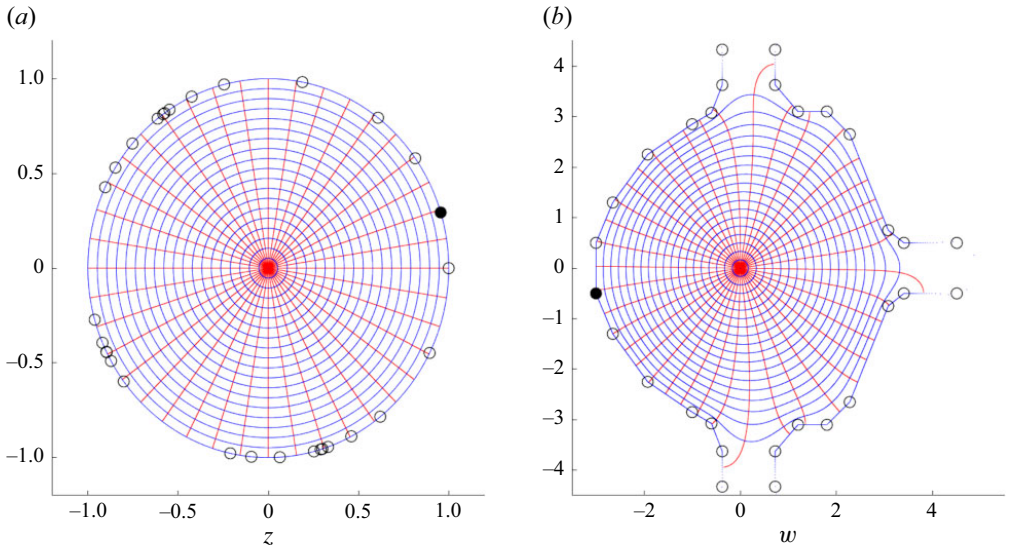


Figure 5. Map $w(z)$ from (a) the disk to (b) the interior of the mixer. The map is illustrated by displaying a regular polar grid in the z domain and visualising its image in the w domain. The vertices and their image in the disk domain are shown as black circles.

described by Trefethen (1980). We outline the complete procedure in Appendix A. Despite adding a numerical step to our procedure, there is still advantage to using this method over simply numerically solving the transport problem from the start. Indeed, the set of pre-vertices z_k only has to be computed once for a given geometry and can then be considered as known. This means that once the problem is solved for a given mixer shape, solutions to our flow and diffusion problem can be generated instantly for any combination of the problem parameters, without requiring additional numerical steps. This is useful in typical microfluidic applications, where the geometry of the mixer is unlikely to change in between experiments.

2.9. *Inverting the map*

Once the parameter problem has been solved and we know the set of parameters z_k, the forward map $w(z)$ can be directly evaluated using (2.9). An illustration of a map to the interior of the mixer is shown in figure 5. However, evaluation of the concentration profile (2.15) for a given point w in the mixer requires an expression of the inverse map $z(w)$. To invert $w(z)$, we differentiate, then take the multiplicative inverse of (2.9). This gives

$$\frac{\mathrm{d}z}{\mathrm{d}w} = \frac{1}{C}\prod_{k=1}^{n}\left(1-\frac{z}{z_k}\right)^{1-\alpha_k}, \tag{2.16}$$

which is an ordinary differential equation (ODE) of the form

$$\frac{\mathrm{d}z}{\mathrm{d}w} = g(w, z). \tag{2.17}$$

This equation can readily be integrated using a prepackaged ODE solver, provided we know the value of $z(w)$ at a given starting point. We use Matlab's prepackaged 'ode45' solver for this calculation, which allows us to get the inverse map everywhere in the domain at a reasonable accuracy. If more accuracy is needed, Newton iterations can be used to

https://doi.org/10.1017/jfm.2025.10840 Published online by Cambridge University Press

refine the map. Newton iterations yield more precise end results, but require a reasonably accurate initial guess, which the ODE solver provides.

2.10. *Complete procedure*

We are now in a position to completely solve the 2-D diffusion problem in our microfluidic mixer. We summarise the steps to obtain analytical flow and concentration profiles in arbitrary polygonal mixers. This sequence is not trivial, as the different maps involved in building the solution require parameters computed in previous steps. The steps are as follows.

(i) Solve the pre-vertice problem for the Schwarz–Christoffel map from the disk to the interior of the mixer.
(ii) Compute the inverse map $z(w)$ on a grid of points in a region of interest.
(iii) From the solution of the pre-vertice problem, obtain the values of z for the inlet and outlet vertices.
(iv) The image of the outlet z_0 allows computation of the Moebius transform (2.10), which gives an expression for $\nu(z)$.
(v) Applying the Moebius transform to the pre-vertices z_1 and z_2 of the inlets gives ν_1 and ν_2, which go in the expression of the complex potential $\Phi(\nu)$, given in (2.11).
(vi) The sequence of transforms $\Phi(\nu)$, $\nu(z)$, $w(z)$ can be combined to evaluate the complex potential $\Phi(w)$ at any point in the interior of the mixer.
(vii) The potential $\Phi(w)$ at any point in the mixer can be substituted in (2.15) to obtain the concentration at that point.

3. Results

3.1. *Streamline plots*

Streamlines in the microfluidic mixer can be plotted in two different ways. The first is to plot the streamlines in the z domain (interior of the disk), using (2.11) and (2.10). Individual points of these streamlines can then be mapped to the interior of the mixer by using the direct transform (2.9). This has the disadvantage of yielding varying resolution in the resulting streamlines, depending on the scale factor at different points in the map. In particular, this method makes it difficult to get accurate streamlines in highly elongated regions such as near the inlets and outlets. The second method of tracing the streamlines is to use the inverse map $z(w)$, which we calculated in § 2.9. Using the inverse map, we can directly find the value of the complex potential $\Phi(\nu(z(w))) = \Phi(w)$ at any given point in the w domain. Provided we have evaluated $z(w)$ for a sufficient number of points in our region of interest, we can then just find the level sets of the real or complex part of $\Phi(w)$ using a built-in function such as Matlab's contour plot. This second method is used to obtain the streamline maps illustrated in figure 6.

3.2. *Concentration plots*

The inverse map $z(w)$ computed in § 2.9 allows us to evaluate the complex potential $\Phi(w)$ for any point in our domain. From this complex potential, we can then evaluate the diffusion solution in the streamline coordinate domain (2.15). This allows us to instantly evaluate the concentration at any given point w in the domain, provided we have already precomputed the inverse map at that point. We use this method to trace concentration maps for various values of the Péclet number, illustrated in figure 7. In figure 8, we show streamline as well as concentration plots obtained for a variety of geometries, reminiscent

https://doi.org/10.1017/jfm.2025.10840 Published online by Cambridge University Press

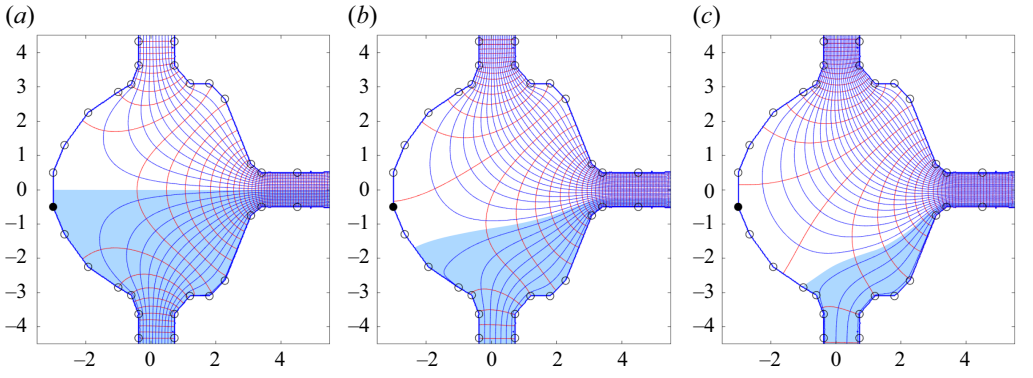


Figure 6. Streamlines (blue) and potential level set (red) in the microfluidic mixer for different ratios of inlet flow rates. The flow from the left inlet has been coloured light blue for additional clarity. (*a*) 1–1 inlet ratio. (*b*) 1–3 inlet ratio. (*c*) 1–8 inlet ratio.

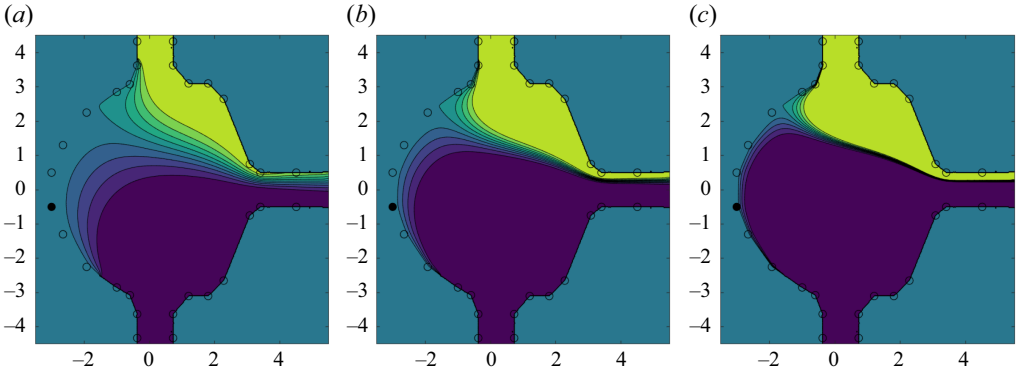


Figure 7. Concentration profile in polygonal mixer with a 1–3 injection ratio for different Péclet number: (*a*) $Pe = 10$; (*b*) $Pe = 100$; (*c*) $Pe = 1000$.

to diverse previously published microfluidic mixers. This showcases the versatility of the approach and its adaptability to arbitrary geometries. Additional figures for multi-inlet mixer geometries are shown in Appendix B.

3.3. *Physical tracer tests*

To validate the results, we compare predicted concentration profiles to experimental physical tracer tests done by injecting blue dye in a microfluidic analogue to an impinging jet mixer. The results are presented in figure 9. We find excellent agreement between predicted and experimental results.

3.4. *Cross-flow geometries*

In addition to mixer geometries, our methodology can be used to model other polygonal microfluidic devices. In particular, cross-flow geometries have been used in a number of microfluidic applications, from the reproduction of G.I. Taylor's classic four-roll mill (Lee *et al.* 2007) to the creation of adjustable hydrodynamic traps (Tanyeri, Johnson-Chavarria & Schroeder 2010) to applications in microrheology (Haward *et al.* 2012). In such systems, alternating inlets and outlets are used to generate tuneable extensional flows in microfluidic chambers. We show in figure 10 how our framework can be used to rapidly

https://doi.org/10.1017/jfm.2025.10840 Published online by Cambridge University Press

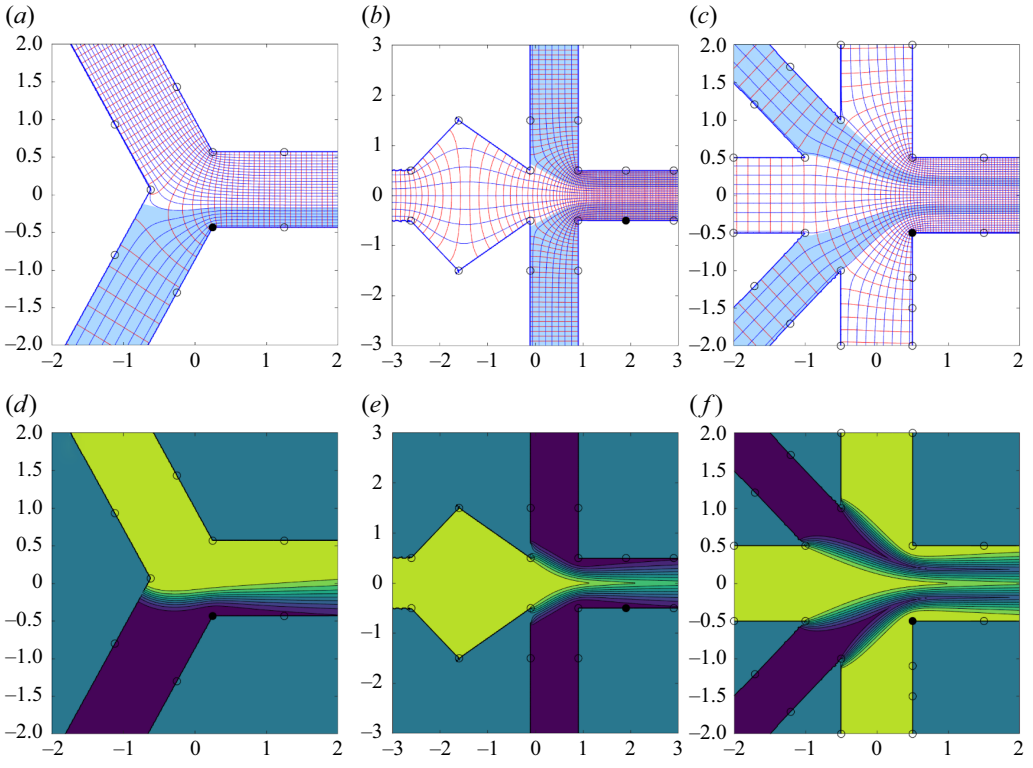


Figure 8. (*a*,*b*,*c*) Streamline profiles and (*d*,*e*,*f*) concentration fields in various polygonal mixers: (*a*,*d*) Y junction with unequal injections (Gobby *et al.* 2001); (*b*,*e*). hydrodynamic focusing reminiscent of (Knight *et al.* 1998); (*c*,*f*) hydrodynamic focusing system with five inlets (Park *et al.* 2006).

model flow and diffusion in one such existing system: the microfluidic rheometry system presented by Haward *et al.* (2012). Analysis of such systems is usually done either by numerically solving the full Stokes flow problem or by only focusing on a region of interest around the stagnation point. Our method provides an elegant alternative, which takes into account the entire geometry and allows for rapid generation of flow or concentration profiles once a map to the interior of the chamber has been found.

4. Discussion

4.1. *Avenues for applications*

One immediate application of the models thus developed is in the determination of residence time distribution curves, which are an important element of the experimental characterisation of chemical reactors (Levenspiel 1998). Neglecting diffusive effects, residence time distribution can be obtained directly by integrating along the streamlines of the flow. Residence time distributions that consider diffusive effects (which are particularly relevant in microfluidic systems, due to the importance of Taylor dispersion) can be obtained by a combination of integration along streamlines in the xy plane and Monte Carlo methods to model diffusion along the z axis, similar to what is done by Houseworth (1984). In systems that are very thin, we expect Taylor dispersion effects to be predominant, which will give heavy tails to residence time distribution curves. While microfluidic systems are often transparent and experimental probing of the flow within

https://doi.org/10.1017/jfm.2025.10840 Published online by Cambridge University Press

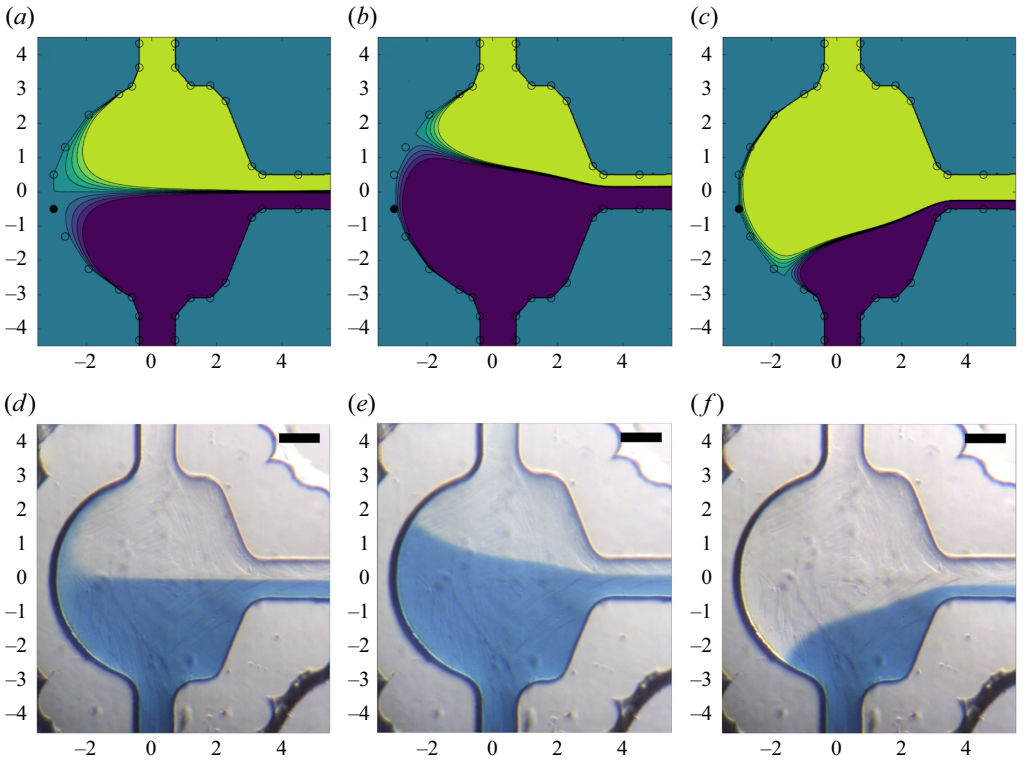


Figure 9. Comparison with physical tracer tests: (*a*,*b*,*c*) predicted concentration profiles for flow ratios of 1–1, 1–1.8 and 3–1, each with Péclet number 1000; (*d*,*e*,*f*) matching physical tracer tests in microfluidic mixer using blue dye. Scale bar, 100 μm.

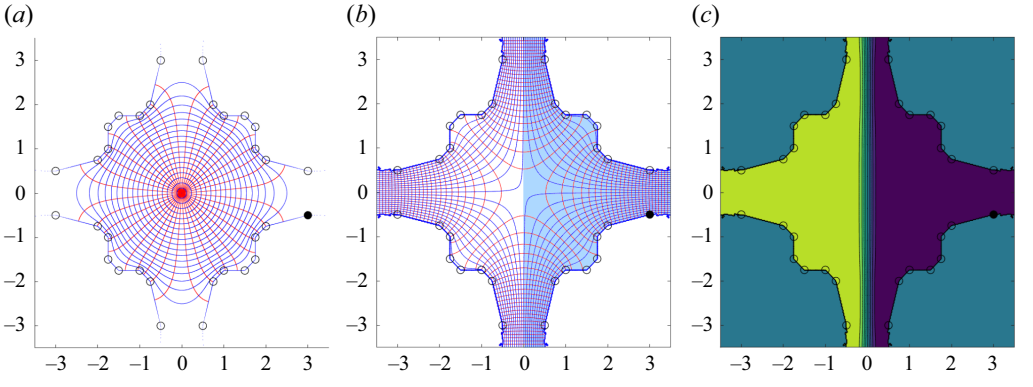


Figure 10. Analysis of an extentional flow rheometry system similar to that of Haward *et al.* (2012). (*a*) Schwarz–Christoffel map to the interior of the chamber. (*b*) Streamline profile for equal injection and aspiration flow rates. (*c*) Resulting concentration profile for $Pe = 50$.

them is better done using techniques such as microparticle image velocimetry (μPIV), the determination of residence time distribution curves is an essential element when probing opaque systems. Computation of residence time distributions may also be a way to extend the methods from the present article to other systems, namely macroscopic flows in groundwatersheds (Haitjema 1995), wetlands (Werner 2000) or river beds (Gooseff *et al.*

https://doi.org/10.1017/jfm.2025.10840 Published online by Cambridge University Press

2011), where the flow may still be approximated using potential flow theory, but direct imaging of the flow by PIV or other visual methods is much more difficult.

Similar Monte Carlo simulations, combined with knowledge of the concentration at every point in the mixer, could be used to simulate the trajectory of individual particles in the mixer and determine their microenvironment at every time step (in a typical flash nanoprecipitation experiment, this could include both the concentration of solvent versus antisolvent as well as the temperature, if the different inlets had different initial temperatures). This precise knowledge could then be combined with the population balance model, or other more elaborate models of particle growth kinetics, to predict the output product in different types of flash nanoprecipitation experiments (Saad & Prud'homme 2016) in microfluidic mixers. This is a crucial next step in the use of microfluidic mixers for pharmaceutical applications, especially for lipid nanoparticles, and will be elaborated on in future publications.

4.2. *Limitations*

The models that we develop in this article hinge on a number of assumptions about our flow profile. In particular, they neglect eventual 3-D effects in the flow. The Hele-Shaw cell formulation is valid at low enough Reynolds numbers and assumes that the flow everywhere can be described by a 2-D potential flow in the xy plane, modulated by a parabolic profile in the z direction. This approximation eventually breaks down in mixers where the height is comparable to the characteristic dimension in the xy plane, as the Reynolds number is increased. This can be seen in analysis of T-mixers, where increasing Reynolds number moves the system from a stratified flow regime first to a vortex regime, where vortices appear along the cross-section, then a so-called engulfment regime, where flow symmetry is broken (Fani, Camarri & Salvetti 2013). Similar effects also lead to trapping of particles in T-junctions (Vigolo, Radl & Stone 2014). These regimes are important to analyse, as mixing is significantly improved in the engulfment regime. However, these are much more difficult to assess analytically, and state-of-the-art models for these situations usually involve a combination of scaling arguments and direct numerical simulation of the Navier–Stokes equations. Similar 3-D effects along the cross-section are also responsible for much of the mixing in many types of chaotic mixers (Stroock *et al.* 2002), which are commonly used in microfluidic mixing experiments. Extensive work on the theoretical foundations of mixing in these 'stretch-and-fold' chaotic mixers have been laid out, and we refer the reader to the pioneering work of Ottino (1989), Ottino & Wiggins (2004) and Aref (1984) for more information on the subject.

4.3. *Possible extensions*

The analytical method developed in this article could be extended in several ways. We mentioned earlier the use of Schwarz–Christoffel maps for the generation of grids, which could then be used to develop numerical methods for the analysis of flow in complex geometries (Thompson, Warsi & Mastin 1982). The method of conformal transforms that we employ is also applicable to some other systems of equations, beyond the simple advection–diffusion in potential flow described throughout this article. In particular, a similar procedure could be applied to dilute electrolyte solutions, in which the concentration field is also affected by a mobility term proportional to the gradient of an electric potential $\boldsymbol{E} = -\boldsymbol{\nabla} V$ (Bazant 2004). In particular, a similar conformal mapping procedure has been used in the study of microfluidic electrodeposition (Gu *et al.* 2022). The method could also be applied to problems of flow and diffusion in porous media, specifically in planar aquifers or in problems of hydrocarbon recovery (Koplik *et al.* 1994).

https://doi.org/10.1017/jfm.2025.10840 Published online by Cambridge University Press

In such problems, our method would allow the precise determination of residence times for Brownian tracers in complex polygonal domains. The method could also easily be extended to domains with variable permeability, using methods outlined by Strack (1988). The extension of the method to problems of transport in porous media also suggests uses in studying transport in hydrogels, porous biological samples or in paper microfluidics (Müller & Clegg 1949; Martinez *et al.* 2007).

The method could very simply be modified to solve problems of steady-advection–diffusion around the exterior of regular polygons. This could yield very interesting results applicable to problems of dissolution (Rycroft & Bazant 2016) or in the analysis of diffusion-limited crystallisation around polygonal grains (Seeger 1953), two areas of transport where similar complex variable methods have been used in the past.

5. Conclusion

We present versatile models for flow and diffusion in microfluidic mixers of arbitrary polygonal shapes, based on Schwarz–Christoffel maps. The models yield values for flow field as well as 2-D-averaged concentration profile everywhere in the geometry. Such models are general and applicable to a range of microfluidic system, in particular, in mixers used for the synthesis of complex nanomaterials, specifically lipid nanoparticles. In this context, a complete knowledge of the microhistory of individual particles (such as is afforded by our models) is a key element in the probing of the kinetics of the particles' self-assembly and should open the way to better knowledge-based methods of synthesis. Beyond this direct application, the mathematical framework we have presented can also find application in other domains, namely transport in porous media, groundwater mechanics or magnetohydrodynamics, to name a few.

6. Method

6.1. *Computation*

Results were generated using custom code written in Matlab R2018a. The nonlinear equation system involved in determining the pre-vertices was solved using the pre-packaged fsolve method. Inversion of the map was performed using the pre-packaged ODE45 solver. Coefficients for the Gauss–Jacobi quadratures, used in calculating the integrals, were determined with custom code using the method of Golub & Welsch (1969).

6.2. *Experimental*

A microfluidic chip which geometrically mimics an impinging jet mixing design was fabricated in polymethyl methacrylate using transition moulding (Parallel Fluidics, USA). The dimensions of the chip are shown in figure 11. Threaded ports were securely bonded to both the inlet and outlet of the chip. The chip's inlet and outlet were connected to fittings (IDEX) and PTFE tubing (inner diameter, 0.5 mm; outer diameter, 1 / 16", IDEX). The inlet tubing was connected to two syringe pumps (SyringeONE NE-1000, New Era Pump Systems Inc.), while the outlet tubing was connected to a waste collection vial. Two solutions were mixed within the microfluidic chip: Milli-Q water and an aqueous solution of Methylene Blue (100 mg L^{-1}). Methylene Blue (minimum 82 % dye content), purchased from Fisher Scientific, was used without further purification. Mixing behaviour was recorded using a colour CMOS camera (DFK 22BUC03, The Imaging Source) mounted on a Nikon Eclipse E20 microscope. The mixing zone was illuminated from below using a halogen light source (HL 150-B) with a flexible arm for optimal positioning. Images were captured at 30 frames per second with a resolution of 1288 $\times$ 922 pixels.

https://doi.org/10.1017/jfm.2025.10840 Published online by Cambridge University Press

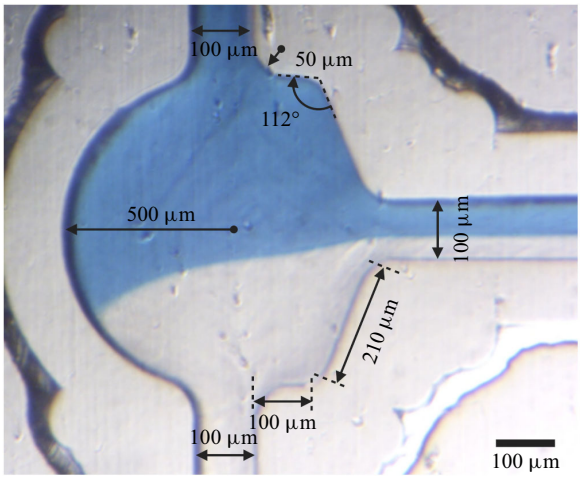


Figure 11. Dimensions of the microfluidic device that mimics an impinging jet mixer design. The depth of the device is 100 μm.

Experiments were run with flow rate ratios varying from 1:1 to 10:1, with an inlet flow rate Q_0 of 25 μl min^{-1}. Using the standard expressions $Re = (\rho u L/\mu)$ and $Pe = (Q_0/2\pi G D)$ gives Reynolds numbers $Re \approx 0.5$ and Péclet numbers $Pe \approx 1000$. We are thus squarely in the low-Reynolds, high-Péclet regime demanded for our approximations to hold.

Funding. This research is funded by the U.S. Food and Drug Administration under the FDA BAA-22-00123 program, Award Number 75F40122C00200. E.B. acknowledges funding from the Fond de Recherche du Quebec, Nature et Technologie (FRQNT) Postdoctoral Fellowship Program, as well as National Science and Engineering Research Council of Canada (NSERC) Postdoctoral Fellowship Program

Declaration of interests. The authors report no conflicts of interest.

Appendix A. Computation of the Schwarz–Christoffel map

The Schwarz–Christoffel map

$$w(z) = w_c + C \int^{z} \prod_{k=1}^{n} \left(1 - \frac{\xi}{z_k}\right)^{\alpha_k - 1} \mathrm{d}\xi \tag{A1}$$

has a number of unknown parameters z_k, which are the image of the vertices of the polygon in the disk domain. These are unknown *a priori* and have to be determined as part of the solution procedure. There are different ways of formulating the parameter problem. We follow the procedure outlined by Trefethen (1980). The Riemann mapping theorem technically lets us freely determine three of the z_k, and some sources fix three pre-vertices and then define $n - 3$ equations to find the other (Driscoll 2002). Instead of doing this, we fix a single one and add an additional condition for the image of the disk's origin. This means we are solving a system of $n - 1$ equations for the pre-vertex problem (instead of $n - 3$ equations if we had fixed three pre-vertices). Doing so allows us to have a better distribution of pre-vertices around the circle and avoid crowding and the numerical instabilities that come with it (see Appendix A.4 for an illustration of this). The equation

https://doi.org/10.1017/jfm.2025.10840 Published online by Cambridge University Press

for the position of the centre point is

$$w_1 - w_c = C \int_0^{z_1} w'(\xi)\, \mathrm{d}\xi. \tag{A2}$$

Equation (A2) is a complex equation, whose real and imaginary part give two real equations for our system. For the remaining $n-3$ equations, we use the polygon's side lengths,

$$\frac{\left|\int_{z_j}^{z_{j+1}} w'(\xi)\, \mathrm{d}\xi\right|}{\left|\int_{z_1}^{z_2} w'(\xi)\, \mathrm{d}\xi\right|} = \frac{|w_{j+1} - w_j|}{|w_2 - w_1|}. \tag{A3}$$

In the case of vertices at infinity (for example, the end of the inlet and outlet channels), we have two infinite side lengths, for which the real (A3) cannot be used. We use instead the complex equation

$$\frac{\int_{z_{j-1}}^{z_{j+1}} w'(\xi)\, \mathrm{d}\xi}{\left|\int_{z_1}^{z_2} w'(\xi)\, \mathrm{d}\xi\right|} = \frac{w_{j+1} - w_{j-1}}{|w_2 - w_1|}, \tag{A4}$$

where w_j is a vertex at infinity. The real and imaginary parts of (A4) give two real equations for each vertex at infinity. Equations A2, A3 and A4 thus give a system of $n-1$ equations which can be solved to obtain the values of z_k, completing the parameter problem. The remaining parameter C can be obtained by normalising with the length of one of the edges. Put succinctly, the pre-vertex problem consists of passing from a description of our geometry in terms of a list of interior angles and side lengths (which is immediately available to us) to one in terms of a list of interior angles and a list of positions of the pre-vertices z_i around the unit circle, which can then be plugged directly in (2.9).

A.1. *Calculating the integrals*

Equation (2.9), which is used to compute the map, as well as (A3) and (A4) used for solving the parameter problem, require the evaluation of complex integrals. Since the function $w(z)$ is analytic everywhere inside of the disk, the value of the integrals is path-independent and we can calculate them along straight line segments. Precise computation of these integrals is difficult when the endpoints are pre-vertices, as the integrand of (2.9) is singular at these points. The presence of singularities at the endpoints of the integrals means traditional Newton–Cotes or Gauss–Legendre quadratures behave very poorly. This is of importance not only in calculating the Schwarz–Christoffel map, but also in solving the pre-vertex problem, as imprecise integrals will also limit the possible precision with which the parameter problem can be solved. Since pre-vertices also have a tendency to crowd in elongated regions (Driscoll 2002), insufficient precision in the integrals can easily lead to parameter problems that fail to converge to a solution. To circumvent this issue, we follow Trefethen (1980) and use compound Gauss–Jacobi quadratures for the integrals with endpoint singularities (Davis & Rabinowitz 2007). The coefficient for these quadratures are obtained by implementing the method of Golub & Welsch (1969), which is based on finding the eigenvalues of a matrix constructed from the recurrence rule of orthogonal polynomials (in this case, Jacobi polynomials). The recurrence rules for Gauss–Jacobi polynomials can be found in classic treatises on orthogonal polynomials (Szego 1939). Variations of Newton–Cotes quadratures that account for the presence of endpoint singularities also exist and could have been used instead (Floryan & Zemach 1988).

https://doi.org/10.1017/jfm.2025.10840 Published online by Cambridge University Press

A.2. *Solving the parameter problem*

Once we have a method for efficient calculation of the integrals, we are almost set to solve the parameter problem. Equations A3 and A4 define a nonlinear algebraic problem. The pre-vertices z_k are distributed around the unit circle and thus can be written as

$$z_k = e^{i\theta_k} \tag{A5}$$

with $0 < \theta_k < 2\pi$ and $\theta_1 < \theta_2 < \ldots < \theta_n$. The problem of the determination of θ_k is thus a constrained one and, as such, is significantly more difficult to solve numerically than an unconstrained one. To bypass this difficulty, Trefethen (1980) suggests the change of variable

$$y_k = \log \frac{\theta_k - \theta_{k-1}}{\theta_{k+1} - \theta_k} \tag{A6}$$

with θ_0 and θ_k taken as 0 and 2π, respectively, both representing the argument of z_k. The passage to an unconstrained nonlinear algebraic problem allows us to use any one of a number of robust 'black-box' numerical solvers. We use Matlab's built-in 'fsolve' function, which is based on a standard algorithm by Powell which combines Newton iterations and steepest descent (Powell 1968). This method allows for the resolution of problems with 30 to 100 vertices in relatively short times, of the order of minutes on a standard laptop computer.

A.3. *Extension to channel geometries*

The method presented previously involves a transformation from a disk domain to the interior of our polygonal mixer. This method yields precise results for the interior of mixers where the dimensions of the domain are comparable in both the x and y directions, but may become unprecise for highly elongated geometries. More specifically, transforming from a disk is not ideal when mapping to long channel-like geometries. Transformation from the disk is also unsuitable for mapping infinite periodic geometries, such as zigzagging channels (Mengeaud, Josserand & Girault 2002) or baffled micromixers (Kimura *et al.* 2018). To model such geometries, it is more appropriate to use an infinite strip as our z domain. Such a map is described by Floryan (1985). The procedure in that case is exactly the same, but the map in (2.9) is replaced with

$$w(z) = w_c + C \int^z \prod_{k=1}^{n} \left(\sinh \frac{\pi}{2} (\xi - z_k) \right)^{\alpha_k - 1} \mathrm{d}\xi. \tag{A7}$$

Additional care must be taken to ensure that, in addition to being correctly ordered, the pre-vertices are on the correct side of the strip. While maps can be found to the interior of 2-D channel-like systems such as zigzag mixers or baffled micromixers, it is important to remember that most of the actual mixing done in these geometries comes not from passive lateral mixing in potential flow, but from effects that are not captured in our current models. Namely, mixing in these geometries depends on 3-D aspects of the flow, on recirculations caused by the interaction of sharp corners and the viscous boundary layers, and on the chaotic aspects of the flow thus generated. That being said, mapping to periodic channel geometries may still be useful for grid generation in the context of numerical analysis, as well as for generating first-order solutions on top of which more complex transport models may be elaborated. For more details on channel geometries, we refer the reader to Floryan (1985), who describes the procedure for channel geometries in detail. We do note that their article uses a different notation from ours, with the pre-vertex domain labelled as w and the physical flow domain as z rather than the other way around.

https://doi.org/10.1017/jfm.2025.10840 Published online by Cambridge University Press

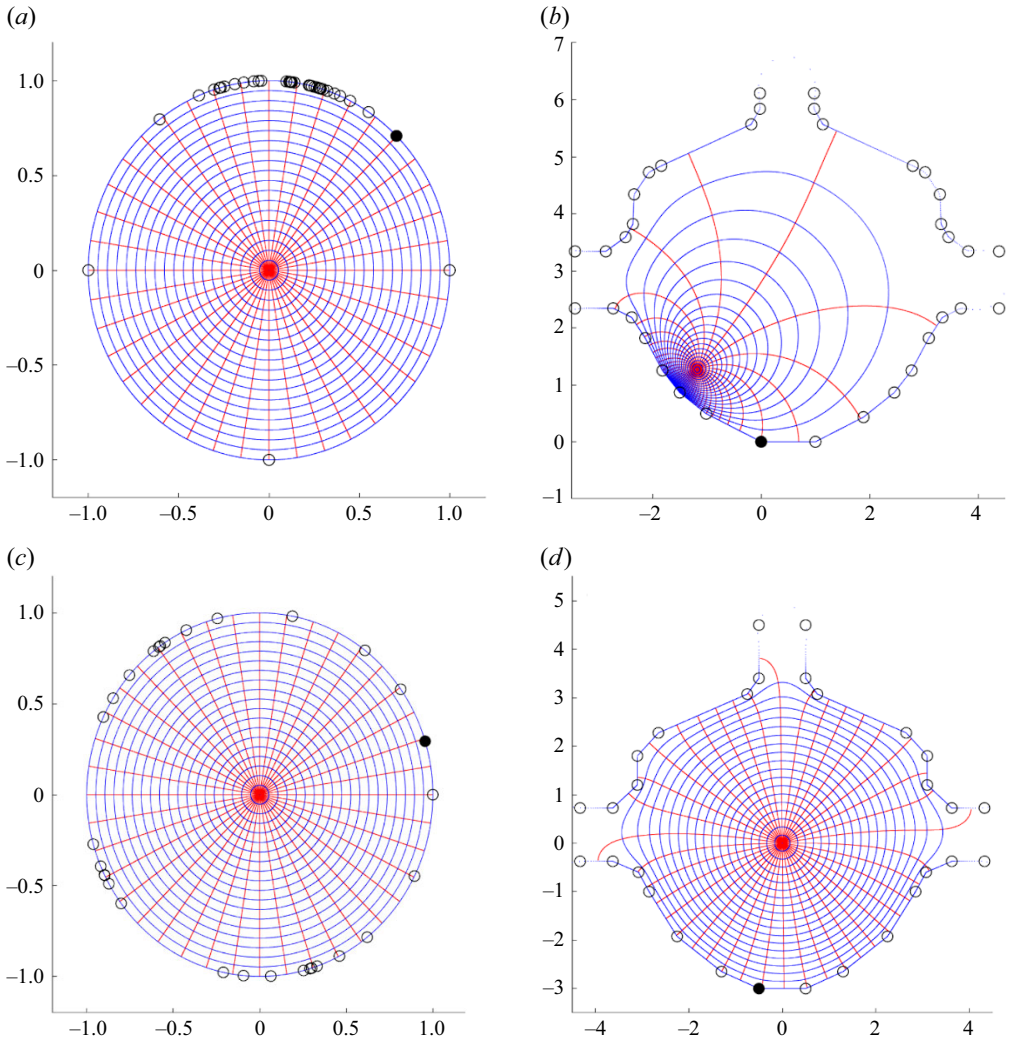


Figure 12. Effect of fixing pre-vertices. (*a*) Disk domain when the position of the last three pre-vertices is fixed at $z_{n-2} = -1$, $z_{n-1} = -i$, $z_n = 1$. (*b*) Map to the interior of the mixer when three pre-vertices are fixed. (*c*) Disk domain when a single pre-vertex is fixed $z_n = 1$ and the image of the origin is prescribed. (*d*) Map to the interior of the mixer when a single vertex and the image of the origin are prescribed.

A.4. *Fixing pre-vertices*

In figure 12, we show an illustration of the effect of the choice of pre-vertices on the Schwarz–Christoffel map. If we fix the position of the last three pre-vertices z_{n-2}, z_{n-1} and z_n, as the Riemann mapping theorem allows us to do, we generally observe heavy crowding of the pre-vertices around the disk (see figure 12*a*), which translates to a map with uneven scale factor, where some regions are very elongated and some are not (figure 12*b*). In contrast, if we fix only a single pre-vertex and add an additional condition for the image of the centre of the disk in the mixer domain, we can obtain a more even distribution of pre-vertices around the circle and a map that is much more uniform (figure 12*c*,*d*), which facilitates both the computation of the pre-vertex problem and the computation of the map and its inverse once the pre-vertex problem has been solved. Somewhat counterintuitively, despite the fact that the second case involves the resolution of a nonlinear system of $n - 1$

https://doi.org/10.1017/jfm.2025.10840 Published online by Cambridge University Press

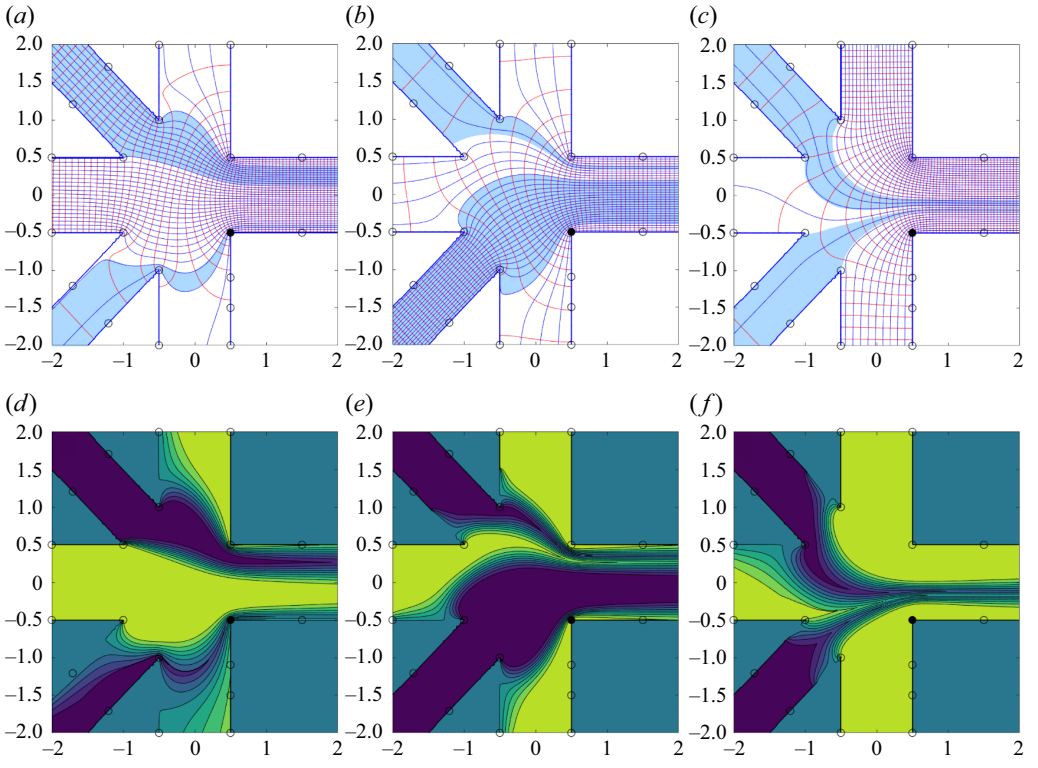


Figure 13. (*a*,*b*,*c*) Streamline and (*d*,*e*,*f*) concentration profiles in multi-inlet mixers for asymmetrical injection ratios.

equations instead of $n-3$ equations, the nonlinear system in the second case may actually converge faster because of the better conditioning of the problem.

Appendix B. Additional figures

In figure 13, we show more results for a multi-inlet solution with asymmetrical inlet injection rates. This shows that our methodology does not hinge on any particular symmetry of the problem.

References

Aref, H. 1984 Stirring by chaotic advection. *J. Fluid Mech.* **143**, 1–21.

Atencia, J. & Beebe, D.J. 2005 Controlled microfluidic interfaces. *Nature* **437** (7059), 648–655.

Batchelor, G.K. 2000 *An Introduction to Fluid Dynamics*. Cambridge University Press.

Bazant, M.Z. 2004 Conformal mapping of some non-harmonic functions in transport theory. *Proc. R. Soc. Lond. Ser. A: Math., Phys. Engng Sci.* **460**(2045), 1433–1452.

Bazant, M.Z. & Moffatt, H.K. 2005 Exact solutions of the Navier–Stokes equations having steady vortex structures. *J. Fluid Mech.* **541**, 55–64.

Boulais, E. & Gervais, T. 2020 Two-dimensional convection–diffusion in multipolar flows with applications in microfluidics and groundwater flow. *Phys. Fluids* **32** (12), 122001.

Boulais, E. & Gervais, T. 2023 The 2D microfluidics cookbook – modeling convection and diffusion in plane flow devices. *Lab Chip* **23** (8), 1967–1980.

Boussinesq, J. 1902 Sur le pouvoir refroidissant d'un courant liquide ou gazeux. *J. Phys. Theor. Appl.* **1** (1), 71–75.

Boyadjian, O., Boulais, E. & Gervais, T. 2022 Microfluidic surface shields: control of flow and diffusion over sensitive surfaces. *Phys. Rev. Appl.* **17** (1), 014012.

https://doi.org/10.1017/jfm.2025.10840 Published online by Cambridge University Press

BRODY, J.P. & YAGER, P. 1997 Diffusion-based extraction in a microfabricated device. *Sensors Actuators A: Phys.* **58** (1), 13–18.

BUSCHMANN, M.D., CARRASCO, M.J., ALISHETTY, S., PAIGE, M., ALAMEH, M.G. & WEISSMAN, D. 2021 Nanomaterial delivery systems for mRNA Vaccines. *Vaccines* **9** (1), 65.

CHEN, D., LIU, Z., GUO, L., YANG, L., ZHAO, Y. & YANG, M. 2025 Controlled preparation of lipid nanoparticles in microreactors: Mixing time, morphology and mRNA delivery. *Chem. Engng J.* **505**, 159318.

CHOI, J., MARGETIS, D., SQUIRES, T.M. & BAZANT, M.Z. 2005 Steady advection–diffusion around finite absorbers in two-dimensional potential flows. *J. Fluid Mech.* **536**, 155–184.

CUMMINGS, L.M., HOHLOV, Y.E., HOWISON, S.D. & KORNEV, K. 1999 Two-dimensional solidification and melting in potential flows. *J. Fluid Mech.* **378**, 1–18.

DAVIS, P.J. & RABINOWITZ, P. 2007 *Methods of Numerical Integration*. Courier Corporation.

DEVOS, C. 2024 Impinging jet mixers: a review of their mixing characteristics, performance considerations, and applications. *AIChE J.* **71**, e18595.

DIAS, F., ELCRAT, A.R. & TREFETHEN, L.N. 1987 Ideal jet flow in two dimensions. *J. Fluid Mech.* **185**, 275–288.

DRISCOLL, T.A. 2002 *Schwarz–Christoffel Mapping*. Cambridge University Press.

EAMES, I. & BUSH, J.W.M. 1999 Longitudinal dispersion by bodies fixed in a potential flow. *Proc. R. Soc. Lond. Ser. A: Mathe., Phys. Engng Sci.* **455** (1990), 3665–3686.

ELCRAT, A.R. & TREFETHEN, L.N. 1986 Classical free-streamline flow over a polygonal obstacle. *J. Comput. Appl. Maths* **14** (1–2), 251–265.

FANI, A., CAMARRI, S. & SALVETTI, M.V. 2013 Investigation of the steady engulfment regime in a three-dimensional T-mixer. *Phys. Fluids* **25** (6), 064102.

FLORYAN, J.M. 1985 Conformal-mapping-based coordinate generation method for channel flows. *J. Comput. Phys.* **58** (2), 229–245.

FLORYAN, J.M. & ZEMACH, C. 1988 Quadrature rules for singular integrals with application to Schwarz–Christoffel mappings. *J. Comput. Phys.* **75** (1), 15–30.

GOBBY, D., ANGELI, P. & GAVRIILIDIS, A. 2001 Mixing characteristics of T-type microfluidic mixers. *J. Micromech. Microengng* **11** (2), 126.

GÖKÇE, O., CASTONGUAY, S., TEMIZ, Y., GERVAIS, T. & DELAMARCHE, E. 2019 Self-coalescing flows in microfluidics for pulse-shaped delivery of reagents. *Nature* **574** (7777), 228–232.

GOLUB, G.H. & WELSCH, J.H. 1969 Calculation of Gauss quadrature rules. *Maths Comput.* **23** (106), 221–230.

GOOSEFF, M.N., BENSON, D.A., BRIGGS, M.A., WEAVER, M., WOLLHEIM, W., PETERSON, B. & HOPKINSON, C.S. 2011 Residence time distributions in surface transient storage zones in streams: estimation via signal deconvolution. *Water Resour. Res.* **47** (5), W05509.

GOYETTE, P.-A., BOULAIS, É., NORMANDEAU, F., LABERGE, G., JUNCKER, D. & GERVAIS, T. 2019 Microfluidic multipoles theory and applications. *Nat. Commun.* **10** (1), 1781.

GU, Z., HUO, P., XU, B., SU, M., BAZANT, M.Z. & DENG, D. 2022 Electrokinetics in two-dimensional complicated geometries: conformal mapping and experimental comparison. *Phys. Rev. Fluids* **7** (3), 033701.

HAITJEMA, H.M. 1995 On the residence time distribution in idealized groundwatersheds. *J. Hydrol.* **172** (1–4), 127–146.

HATCH, A., KAMHOLZ, A.E., HAWKINS, K.R., MUNSON, M.S., SCHILLING, E.A., WEIGL, B.H. & YAGER, P. 2001 A rapid diffusion immunoassay in a T-sensor. *Nat. Biotechnol.* **19** (5), 461–465.

HAWARD, S.J., OLIVEIRA, M.S.N., ALVES, M.A. & MCKINLEY, G.H. 2012 Optimized cross-slot flow geometry for microfluidic extensional rheometry. *Phys. Rev. Lett.* **109** (12), 128301.

HOUSEWORTH, J.E. 1984 Shear dispersion and residence time for Laminar flow in capillary tubes. *J. Fluid Mech.* **142**, 289–308.

HUNT, J.C.R. 1973 A theory of turbulent flow round two-dimensional bluff bodies. *J. Fluid Mech.* **61** (4), 625–706.

HUNT, J.C.R. & MULHEARN, P.J. 1973 Turbulent dispersion from sources near two-dimensional obstacles. *J. Fluid Mech.* **61** (2), 245–274.

JAHN, A., VREELAND, W.N., DEVOE, D.L., LOCASCIO, L.E. & GAITAN, M. 2007 Microfluidic directed formation of liposomes of controlled size. *Langmuir* **23** (11), 6289–6293.

KAMHOLZ, A.E., WEIGL, B.H., FINLAYSON, B.A. & YAGER, P. 1999 Quantitative analysis of molecular interaction in a microfluidic channel: the T-sensor. *Anal. Chem.* **71** (23), 5340–5347.

KIMURA, N., MAEKI, M., SATO, Y., NOTE, Y., ISHIDA, A., TANI, H., HARASHIMA, H. & TOKESHI, M. 2018 Development of the iLiNP device: fine tuning the lipid nanoparticle size within 10 nm for drug delivery. *ACS Omega* **3** (5), 5044–5051.

https://doi.org/10.1017/jfm.2025.10840 Published online by Cambridge University Press

KNIGHT, J.B., VISHWANATH, A., BRODY, J.P. & AUSTIN, R.H. 1998 Hydrodynamic focusing on a silicon chip: mixing nanoliters in microseconds. *Phys. Rev. Lett.* **80** (17), 3863.
KOPLIK, J., REDNER, S. & HINCH, E.J. 1994 Tracer dispersion in planar multipole flows. *Phys. Rev. E* **50** (6), 4650.
KRZYSZTOŃ, R., SALEM, B., LEE, D.J., SCHWAKE, G., WAGNER, E. & RÄDLER, J.O. 2017 Microfluidic self-assembly of folate-targeted monomolecular siRNA-lipid nanoparticles. *Nanoscale* **9** (22), 7442–7453.
LAMB, H. 1924 *Hydrodynamics*. Cambridge University Press.
LASIC, D.D., JOANNIC, R., KELLER, B.C., FREDERIK, P.M. & AUVRAY, L. 2001 Spontaneous vesiculation. *Adv. Colloid Interface* **89**, 337–349.
LEE, J.S., DYLLA-SPEARS, R., TECLEMARIAM, N.P. & MULLER, S.J. 2007 Microfluidic four-roll mill for all flow types. *Appl. Phys. Lett.* **90** (7), 074103.
LENG, J., EGELHAAF, S.U. & CATES, M.E. 2003 Kinetics of the micelle-to-vesicle transition: aqueous Lecithin-bile salt mixtures. *Biophys. J.* **85** (3), 1624–1646.
LEVENSPIEL, O. 1998 *Chemical Reaction Engineering*. 3rd edn. John Wiley & Sons.
MARSHALL, D.E. & ROHDE, S. 2007 Convergence of a variant of the zipper algorithm for conformal mapping. *SIAM J. Numer. Anal.* **45** (6), 2577–2609.
MARTINEZ, A.W., PHILLIPS, S.T., BUTTE, M.J. & WHITESIDES, G.M. 2007 Patterned paper as a platform for inexpensive, low-volume, portable bioassays. *Angewandte Chemie* **119** (8), 1340–1342.
MCKEE, K.I. 2024 Magnetohydrodynamic flow control in Hele–Shaw cells. *J. Fluid Mech.* **993**, A11.
MENGEAUD, V., JOSSERAND, J. & GIRAULT, H.H. 2002 Mixing processes in a zigzag microchannel: finite element simulations and optical study. *Anal. Chem.* **74** (16), 4279–4286.
MENIKOFF, R. & ZEMACH, C. 1980 Methods for numerical conformal mapping. *J. Comput. Phys.* **36** (3), 366–410.
METCALFE, G., LESTER, D., ORD, A., KULKARNI, P., RUDMAN, M., TREFRY, M., HOBBS, B., REGENAUR-LIEB, K. & MORRIS, J. 2010 An experimental and theoretical study of the mixing characteristics of a periodically reoriented irrotational flow. *Phil. Trans. R. Soc. A: Math., Phys. Engng Sci.* **368** (1918), 2147–2162.
MILNE-THOMSON, L.M. 1943 *Theoretical Hydrodynamics*. Courier Corporation.
MÜLLER, R.H. & CLEGG, D.L. 1949 Automatic paper chromatography. *Anal. Chem.* **21** (9), 1123–1125.
OTTINO, J.M. 1989 *The Kinematics of Mixing: Stretching, Chaos, and Transport*. vol. 3. UK: Cambridge University Press.
OTTINO, J.M. & WIGGINS, S. 2004 Introduction: mixing in microfluidics. *Phil. Trans. R. Soc. Lond. Ser. A: Math., Phys. Engng Sci.* **362** (1818), 923–935.
LARAMY, O'.B., *et al.* 2023 Process robustness in lipid nanoparticle production: a comparison of microfluidic and turbulent jet mixing. *Mol. Pharm.* **20** (8), 4285–4296.
PARK, H.Y., QIU, X., RHOADES, E., KORLACH, J., KWOK, L.W., ZIPFEL, W.R., WEBB, W.W. & POLLACK, L. 2006 Achieving uniform mixing in a microfluidic device: hydrodynamic focusing prior to mixing. *Anal. Chem.* **78** (13), 4465–4473.
PEARSON, C.E. 1957 On the finite strip problem. *Q. Appl. Maths* **15** (2), 203–208.
PEETERS, D. & HUYSKENS, P. 1993 Endothermicity or exothermicity of water/alcohol mixtures. *J. Mol. Struct.* **300**, 539–550.
PETERSEN, D.M.S., CHAUDHARY, N., ARRAL, M.L., WEISS, R.M. & WHITEHEAD, K.A. 2023 The mixing method used to formulate lipid nanoparticles affects mrna delivery efficacy and organ tropism. *Eur. J. Pharm. Biopharm.* **192**, 126–135.
POWELL, M.J.D. 1968 A Fortran subroutine for solving systems of nonlinear algebraic equations. *Tech. Rep.*Atomic Energy Research Establishment, Harwell, England (United Kingdom).
RYCROFT, C.H. & BAZANT, M.Z. 2016 Asymmetric collapse by dissolution or melting in a uniform flow. *Proc. R. Soc. A: Math., Phys. Engng Sci.* **472** (2185), 20150531.
SAAD, W.S. & PRUD'HOMME, R.K. 2016 Principles of nanoparticle formation by flash nanoprecipitation. *Nano Today* **11** (2), 212–227.
SCHNEIDER, T.M., MANDRE, S. & BRENNER, M.P. 2011 Algorithm for a microfluidic assembly line. *Phys. Rev. Lett.* **106** (9), 094503.
SEEGER, A. 1953 I. Diffusion problems associated with the growth of crystals from dilute solution. *Lond., Edin., Dublin Phil. Mag. J. Sci.* **44** (348), 1–13.
SMITH, E.A. 1996 Pressure and velocity of air during drying and storage of cereal grains. *Transport Porous Med.* **23**, 197–218.
STEPHENSON, K. 2005 *Introduction to Circle Packing: The Theory of Discrete Analytic Functions*. Cambridge University Press.
STRACK, O.D.L. 1988 *Groundwater Mechanics*. Prentice-Hall, Inc.

https://doi.org/10.1017/jfm.2025.10840 Published online by Cambridge University Press

STROOCK, A.D., DERTINGER, S.K.W., AJDARI, A., MEZIC, I., STONE, H.A. & WHITESIDES, G.M. 2002 Chaotic mixer for microchannels. *Science* **295** (5555), 647–651.

VAN SWAAY, D. & DEMELLO, A. 2013 Microfluidic methods for forming liposomes. *Lab Chip* **13** (5), 752–767.

SZEGO, G. 1939 *Orthogonal Polynomials*. American Mathematical Society.

TANYERI, M., JOHNSON-CHAVARRIA, E.M. & SCHROEDER, C.M. 2010 Hydrodynamic trap for single particles and cells. *Appl. Phys. Lett.* **96** (22), 224101.

THOMPSON, J.F., WARSI, Z.U.A. & WAYNE MASTIN, C. 1982 Boundary-fitted coordinate systems for numerical solution of partial differential equations—A review. *J. Comput. Phys.* **47** (1), 1–108.

TREFETHEN, L.N. 1980 Numerical computation of the schwarz–Christoffel transformation. *SIAM J. Scientifi Statist. Comput.* **1** (1), 82–102.

VIGOLO, D., RADL, S. & STONE, H.A. 2014 Unexpected trapping of particles at a T junction. *Proc. Natl Acad. Sci.* **111** (13), 4770–4775.

WEIGL, B.H. & YAGER, P. 1999 Microfluidic diffusion-based separation and detection. *Science* **283** (5400), 346–347.

WERNER, T.M. & KADLEC, R.H. 2000 Wetland residence time distribution modeling. *Ecol. Engng* **15** (1–2), 77–90.

ZOUACHE, M.A., EAMES, I. & LUTHERT, P.J. 2015 Blood flow in the choriocapillaris. *J. Fluid Mech.* **774**, 37–66.

https://doi.org/10.1017/jfm.2025.10840 Published online by Cambridge University Press